Resistance to antiangiogenic therapy is directed by vascular phenotype, vessel stabilization, and maturation in malignant melanoma

Iris Helfrich,[1,3,4] Inka Scheffrahn,[2] Sönke Bartling,[5] Joachim Weis,[6] Verena von Felbert,[6] Mark Middleton,[7] Masahi Kato,[8] Süleyman Ergün,[2] and Dirk Schadendorf[1]

[1]Department of Dermatology and [2]Institute of Anatomy, University Hospital Essen, D-45122 Essen, Germany
[3]Joint Research Division of Vascular Biology, Medical Faculty Mannheim, University of Heidelberg, D-68167 Mannheim, Germany
[4]Joint Research Division of Vascular Biology and [5]Medical Physics in Radiology, German Cancer Research Center, D-69120 Heidelberg, Germany
[6]Institute for Neuropathology, Medical Faculty, RWTH Aachen University, 52074 Aachen, Germany
[7]University of Oxford, Department of Medical Oncology, Churchill Hospital, OX3 7LJ Oxford, England, UK
[8]Unit of Environmental Health Sciences, Department of Biomedical Sciences, College of Life and Health Sciences, Chubu University, Kasugai-shi, 487-8501 Aichi, Japan

Angiogenesis is not only dependent on endothelial cell invasion and proliferation, it also requires pericyte coverage of vascular sprouts for stabilization of vascular walls. Clinical efficacy of angiogenesis inhibitors targeting the vascular endothelial growth factor (VEGF) signaling pathway is still limited to date. We hypothesized that the level of vessel maturation is critically involved in the response to antiangiogenic therapies. To test this hypothesis, we evaluated the vascular network in spontaneously developing melanomas of MT/*ret* transgenic mice after using PTK787/ZK222584 for anti–VEGF therapy but also analyzed human melanoma metastases taken at clinical relapse in patients undergoing adjuvant treatment using bevacizumab. Both experimental settings showed that tumor vessels, which are resistant to anti–VEGF therapy, are characterized by enhanced vessel diameter and normalization of the vascular bed by coverage of mature pericytes and immunoreactivity for desmin, NG-2, platelet–derived growth factor receptor β, and the late-stage maturity marker α smooth muscle actin. Our findings emphasize that the level of mural cell differentiation and stabilization of the vascular wall significantly contribute to the response toward antiangiogenic therapy in melanoma. This study may be useful in paving the way toward a more rational development of second generation antiangiogenic combination therapies and in providing, for the first time, a murine model to study this.

CORRESPONDENCE
Dirk Schadendorf:
dirk.schadendorf@uk-essen.de
OR
Iris Helfrich:
iris.helfrich@uk-essen.de

Abbreviations used: Ang, angiopoietin; cDNA, complementary DNA; fl-VCT, flat-panel volume computer tomography; MVD, microvessel density; PDGF, platelet–derived growth factor; PDGFR, PDGF receptor; PTK/ZK, PTK787/ZK222584; SMA, smooth muscle actin; TRP, tyrosinase-related protein; VEGF, vascular endothelial growth factor; VEGFR, VEGF receptor.

Angiogenesis is a pivotal process for growth, invasion, and spread of tumors and is therefore used as a therapeutic target in many types of cancer (Hanahan and Folkman, 1996; Ferrara and Kerbel, 2005). Sprouting of capillaries from preexisting blood vessels is accomplished by a hypoxia-driven mechanism, within which vascular endothelial growth factor (VEGF) A has been identified as the most potent inducer of the angiogenic cascade (Neufeld et al., 1999). Several strategies against VEGF-A (Siemeister et al., 1998; W. Leenders et al., 2002; Ferrara et al., 2004) or its receptor, VEGF receptor (VEGFR) 1 (Flt-1), and its major signaling receptor, VEGFR-2 (KDR/Flk-1; Kunkel et al., 2001; Sweeney et al., 2002), have been de-

veloped including neutralizing humanized antibodies. Another way to efficiently perturb VEGF-A signaling is to block the kinase activity of VEGFRs by small-molecule inhibitors, such as sorafenib, sunitinib, or PTK787/ZK222584 (PTK/ZK; Hess-Stumpp et al., 2005; Escudier et al., 2007; Thomas et al., 2007). VEGF directly stimulates endothelial cell proliferation and migration, but its role in pericyte biology is still unclear and controversial. The interplay of platelet–derived growth factor (PDGF) B,

The Journal of Experimental Medicine

which is secreted by endothelial cells, and pericytes, expressing PDGF receptor (PDGFR) β, is important for mural cell recruitment during development (Hellström et al., 1999; Armulik et al., 2005; Betsholtz et al., 2005; Carmeliet 2005; von Tell et al., 2006; Andrae et al., 2008). The absence of pericytes, which play a key role in vascular development, vessel stabilization, maturation, and remodeling, is thought to be at least partially responsible for the irregular, tortuous, and leaky blood vessels found within tumors (Morikawa et al., 2002; Abramsson et al., 2003). These later steps of the angiogenic cascade are controlled by the PDGFs and angiopoietins (Ang's; Fiedler and Augustin, 2006; Andrae et al., 2008). Ang-2, which is expressed by endothelia cells (Fiedler et al., 2004), acts as a context-specific antagonist of Ang-1/Tie2 signaling. As such, it destabilizes the quiescent endothelial cell layer lining the vessel lumina and increases vascular leakage (Carlson et al., 2001) but its effects appear to be contextual and dependent on local cytokine milieu (Hanahan 1997), particularly on the presence of VEGF. The benefits of targeting both pericytes and endothelial cells in tumor vessels have been shown in several tumor models (Bergers et al., 2003; Erber et al., 2004), and receptor tyrosine kinase inhibitors that block both VEGFRs and PDGFRs have been shown to be more efficacious in combination than in single use (Bergers et al., 2003; Erber et al., 2004). Although systematic studies have provided ample evidence that tumor progression correlates with tumor-induced angiogenesis, this issue remains controversial in the case of human cutaneous melanoma (Folkman et al., 1989; Fallowfield and Cook, 1991; Ilmonen et al., 1999). Neovascularization has been considered to be synonymous with directed vessel ingrowth in almost all of these studies, but alternative growth factor–independent mechanisms have been reported, both experimentally and in human tumors (Paku 1998). It has been shown for some human cancers, including non–small cell lung carcinomas (Pezzella et al., 1997) and human glioma (Holash et al., 1999), that tumors in more natural settings do not always originate avascularly, particularly when they arise within or metastasize to vascularized tissue. In such settings, tumor cells have the ability to incorporate (i.e., co-opt) host vessels (W.P. Leenders et al., 2002), which has also been shown as an important mechanism during development of cutaneous melanoma (Döme et al., 2002) and melanoma of the brain (Küsters et al., 2002). This leads to the speculation that although compounds may be efficient inhibitors of angiogenesis and tumor growth in angiogenesis–dependent tumors, their effects may be limited in growth factor–independent tumors using mature vessels. The present study analyzed the vascular network and levels of pericyte-mediated vessel maturation in human melanoma metastases and melanomas of a corresponding tumor model grown during anti-VEGF therapy. In this paper, first, we identify the spontaneous endogenously driven murine melanoma model (MT/*ret*) as the first existing model where VEGF–dependent and independent tumor growth occurs in parallel, and, second, we provide strong evidence that the level of mural cell differentiation influencing vessel maturation and pericyte coverage is essential for

vessel stabilization and crucial factors sensitizing blood vessels to anti-VEGF therapy, both in melanoma patients and in the corresponding murine tumor model.

RESULTS

Tumor growth and progression in MT/ret transgenic mice occurs via high, but also low, angiogenic–active vascularization

For analysis of tumor angiogenesis in a physiological setting, we used MT/*ret* transgenic mice, which spontaneously develop multiple melanoma (Kato et al., 1998) and metastases in lymph nodes (100%), spleen (>80%), and lung and brain (>10%; Fig. S1 A). Tumor development started after a short latency of 2–3 wk in the face and on the back of these mice, with up to ∼100 tumors/mouse (∼20% ± SD) by the age of 9–10 wk (unpublished data). Immunohistological analyses revealed morphological analogy to human melanoma (unpublished data) and the expression of tyrosinase, tyrosinase–related protein (TRP) 1, and gp-100, which are enzymes, regulating the quality and quantity of pigment production in melanocytes (Fig. S1 B). Interestingly, detailed studies on tumor vascular beds showed two different vascular phenotypes in this tumor model (Fig. 1, A and B). One predominant type showed a high angiogenic–active phenotype (Fig. 1 A) with a mean microvessel density (MVD) of 250/mm^2 (Fig. 1 C), in contrast to a second type which is characterized by only a few intratumoral vessels (Fig. 1 B) and a mean MVD of 40/mm^2 (Fig. 1 C) and which was subsequently described as low angiogenic tumor. Analyzing tumor volume in relation to MVD, it became evident that the phenotype of the vascular network in MT/*ret* melanoma was dependent on neither tumor volume nor tumor location (Fig. 1 C and not depicted). Furthermore, the intratumoral vessels of the low angiogenic tumors showed an almost 10-fold increase in vessel perimeter in comparison with the vessels of the high angiogenic tumor type (Fig. 1 D) and a significant increase (P ≤ 0.001) in vessel lumina (not depicted). In contrast to high angiogenic tumors, total coverage by endothelial cells in the peritumoral tissue area of low angiogenic-active tumor nodules was observed (Fig. 1 B, arrowhead).

In addition, lymphatic endothelial cells were detected in a high number of tumor septa and peritumoral areas but not in intratumoral tissue in both tumor types (Fig. S1 C). Assessment of the relative abundance of the vascular bed phenotype per mouse showed a mean distribution of 83% high angiogenic to 17% low angiogenic tumors (Fig. 1 E). However, vessel perfusion did not differ in either tumor type (Fig. 1 F). Assessment of vessel–vessel distance in individual nodules revealed a mean distance of 41.8 μm (±19.1 μm) in tumors with high-angiogenic potential in comparison with 172.2 μm (±57.7 μm) in low angiogenic-active tumors (Fig. 1 G), which warrant the delivery of oxygen and nutrients for growth and progression.

Rapid tumor growth of high angiogenic tumors results in increased tumor hypoxia

The observations described in the previous section strongly suggest that both vascular beds coexist in parallel in the MT/*ret* transgenic model without the need to switch from the low- to

the high angiogenic vascular phenotype to grow. To address potential differences in the tumor growth kinetic, we measured tumor volume of individual nodules starting early in life with tumor-free mice at weekly intervals over a period of 4 wk using flat-panel volume computer tomography (fl-VCT). Over the first 3 wk, tumor growth kinetics of high angiogenic-active tumors were significantly increased (P ≤ 0.001) compared with tumors with low vessel density (Fig. 2 A). This was paralleled by increased expression of the proliferation marker Ki-67 (Fig. 2 B) and apoptosis indices (not depicted) in high angiogenic tumors, associated with increased intratumoral hypoxic regions in those tumors (Fig. 2, C and D). The distribution of hypoxic areas within both vascular beds was paralleled by detection of glutase-1 (unpublished data).

Lack of pericyte coverage and defects in vessel maturation promote neovascularization in angiogenic tumors of MT/ret transgenic mice

It has been shown that a plasticity window for remodeling neovasculature is defined by pericyte coverage (Benjamin et al., 1998). Therefore, we consequently analyzed the recruitment of mural cells in both vascular phenotypes. NG-2, Desmin, and PDGFR-β have been established as markers of early, i.e., immature, pericytes, whereas α smooth muscle actin (SMA) has been reported as a marker of mature mural cells including pericytes and smooth muscle cells (Nehls et al., 1992; Morikawa et al., 2002; Gerhardt and Betsholtz, 2003). Intratumoral microvessels of MT/ret transgenic melanoma were covered by Desmin–positive mural cells without significant difference in both vascularization phenotypes (80% in high angiogenic vs. 92% in low angiogenic tumors; Fig. 3, A and B). A comparable percentage of vessels also expressed the early markers NG-2 and PDGFR-β (Fig. 3 B). In contrast, coverage of intratumoral microvessels by α–SMA–positive mural cells was significantly higher (P ≤ 0.001) in tumors of low vessel density (98%) compared with high angiogenic-active tumors (2%; Fig. 3, B and C). In accordance with the maturation defect and partial lack of pericyte coverage, excessive vessel leakiness was observed in tumors of high vessel density using FITC-conjugated dextran (unpublished data). Alongside the
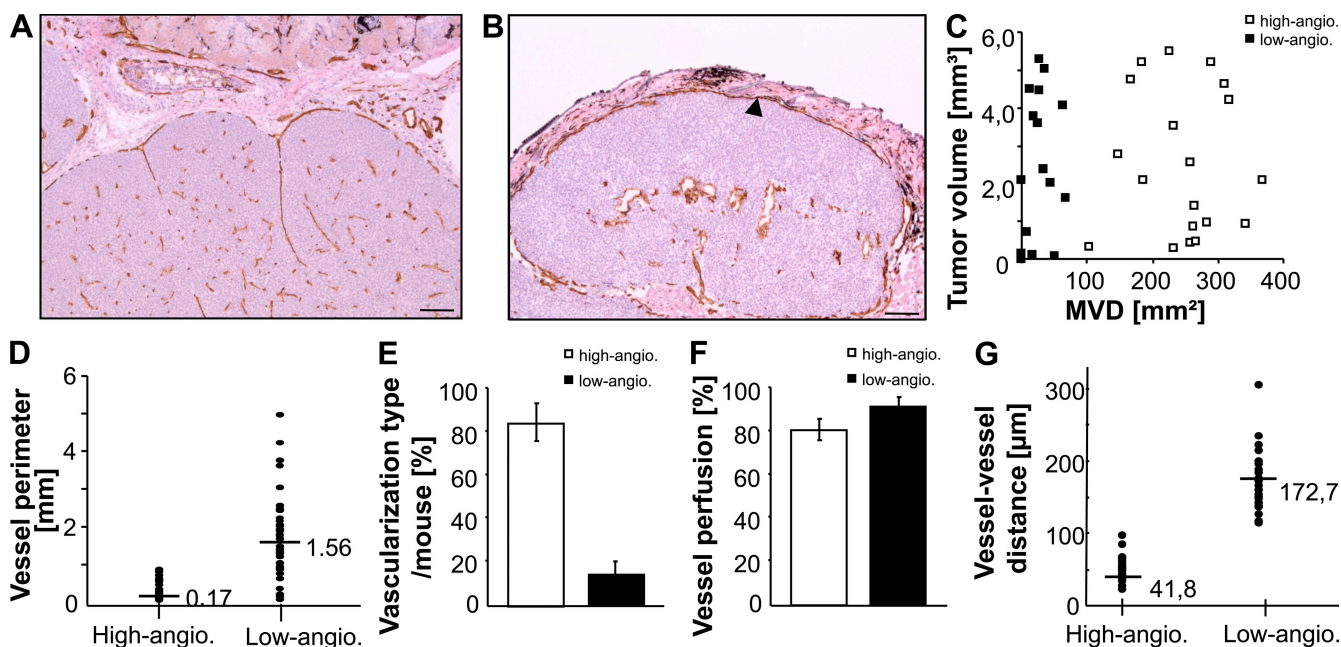

Figure 1. **Immunohistological and morphometric analyses of the vascular network in melanoma of MT/ret transgenic mice.** (A and B) Representative images for immunoperoxidase detection of blood vessels using the endothelial marker CD31 in melanoma of high angiogenic (A) and low angiogenic (B) potential (n = 478 tumors of 63 mice, independently performed). Arrowheads indicate peritumoral coverage of endothelial cells in low angiogenic tumors. (C) Scatter blot for MVD (in millimeters squared) versus tumor volume (in millimeters cubed) in high and low angiogenic tumors (n = 20 tumors/vascular bed of four mice). (D) Quantification of vessel perimeter (in millimeters) for both vascular beds of MT/ret transgenic melanoma (n = 500 intratumoral vessels [100 vessels/tumor] of five high angiogenic and 100 intratumoral vessels of nine low angiogenic tumors isolated from two mice). (E) Immunohistochemically based distribution analyses for the incidence of high and low angiogenic-active tumors per mouse (in percentage) calculated after isolation of all tumors (n = 478 tumors of five mice). (F) Perfusion analysis (in percentage) of intratumoral vessels was performed after injection of FITC-conjugated lectin into tumor-bearing mice. Analyzing the number of double-positive lectin- and CD31-positive tumor vessels in comparison with CD31 single-stained vessels resulted in calculation of vessel perfusion (n = 100 vessels/vascular phenotype in 10 tumors each of four mice). Injection experiments were independently performed in each mouse. (G) Analysis of vessel–vessel distances (in micrometers) in both vascular beds of MT/ret-transgenic melanoma (n = 500 intratumoral vessels [100 vessels/tumor] of five high angiogenic and 100 intratumoral vessels of nine low angiogenic tumors of two mice). Median values of the experimental groups are indicated by the horizontal lines (D and G). All morphometric analyzes were microscopically quantified using CD31-stained tissue sections. Error bars, mean ± SD. Bars, 50 μm.

Figure 3. **Quantitative assessment of mural cell maturation and stabilization in MT/*ret* melanoma.** (A and C) Immunohistochemical double staining for the endothelial marker CD31 (green) and the early pericytic marker Desmin (red) in low-vascularized (I) and high-vascularized (II) tumors (A), as well as for the late differentiation marker α-SMA (C; red). Representative images of >10 independently performed experiments are presented (n = 43 high angiogenic and 27 low angiogenic tumors of four mice). (B) Quantification of vessel coverage, calculated as the percentage of NG-2–, Desmin–, PDGFR-β–, or α-SMA–positive cells compared with the number of CD31-positive vessels (n = 1,087 high angiogenic and 352 low angiogenic tumor vessels of 10 tumors of four mice; ***, P ≤ 0.001). Data are collected from >10 independent experiments. (D and E) Electron microscopic evaluation of the vascular wall structure in sections of tumor tissues with high vascular density (two to three blood vessels per microscopic field; D) and low vascular density (one to two blood vessels in three to four microscopic fields; E), analyzed for their construction of a basal laminar, availability of pericytes, and pericyte integration (n = 9 tumors/vascular bed of three mice). Data are representative of three independent experiments. EC, endothelial cell; Ery, erythrocytes within the vessel lumen; TC, tumor cells; star, pericyte; arrowheads, basal lamina. Representative images are presented (A and C–E). Error bars, mean ± SD. Bars: (A and C) 100 μm; (D and E) 2 μm.

in high angiogenic tumors, which in turn may result in enhanced sensitivity of intratumoral microvessels to anti-VEGF therapy. We therefore analyzed the expression of Ang–1, which induces Tie2 activation leading to vessel stabilization and maturation (Wong et al., 1997), of its antagonist and vessel destabilization factor Ang–2, of their receptor Tie2, and of VEGF-A and its main receptor VEGFR2 in laser microdissected intratumoral endothelial cells by quantitative real–time PCR. A significant reduction (P ≤ 0.001) in expression of all monitored factors was observed in low angiogenic-active endothelial cells, except for levels of Ang–1, which was present in equal amounts in both vascular beds. In detail, intratumoral endothelial cells of low angiogenic tumors showed an ∼100-fold decrease in expression of Ang–2 and its receptor Tie2, as well as an ∼1,000-fold reduction of VEGF-A and its major receptor VEGFR2 compared with endothelial cells isolated from angiogenic-active vessels (Fig. 4). bEnd3 cells, a mouse endothelial cell line derived from cortex blood vessels, mouse heart, and brain were used as controls for the angiogenic factor expression.

PTK/ZK does not affect mature tumor vasculature in MT/ret melanoma

Pericytes, in particular, have been recently appreciated as critical regulators of vessel formation, stabilization, and function (Armulik et al., 2005; von Tell et al., 2006), but their role in the susceptibility of tumor vasculature to antiangiogenic therapy has not been finally clarified. Based on the observations described in the previous section, we used the MT/ret

model because it represents two different vascular beds with differences in vessel maturation and stabilization to study sensitivity to anti-VEGF therapy. As a reference for an antiangiogenic therapy, we used PTK/ZK, a small molecule tyrosine kinase inhibitor, which was shown to specifically block VEGF-induced autophosphorylation of VEGFR–1, –2, and –3 and to inhibit endothelial cell proliferation, differentiation, and tumor angiogenesis (Wood et al., 2000; Hess-Stumpp et al., 2005). Oral administration of PTK/ZK in tumor-free MT/ret transgenic mice resulted in an excessive reduction (P ≤ 0.001) of tumor numbers (Fig. 5, A and B) without affecting the volume of growing tumors compared with the vehicle-treated control group (Fig. 5 C). Histological analyses disclosed that nearly all tumors (mean, 98%) that developed during PTK/ZK treatment exhibited the low angiogenic vascular phenotype (Fig. S2, A and B). As expected, the vehicle-treated control group exhibited the normal distribution of ∼80% high versus 20% low angiogenic-active tumor beds (Fig. S2 B).

PTK/ZK efficiency represses tumor angiogenesis and results in vessel regression

We consequently analyzed the therapeutic effect of anti-VEGF therapy using PTK/ZK in tumor-bearing animals to address the question of whether PTK/ZK is only able to inhibit endothelial cell recruitment during sprouting angiogenesis or whether PTK/ZK is also able to affect intratumoral vascularization of existing tumors. For this purpose, tumor-bearing MT/ret transgenic mice were selected for a therapeutic intervention trial and individually screened for tumor number and volume at
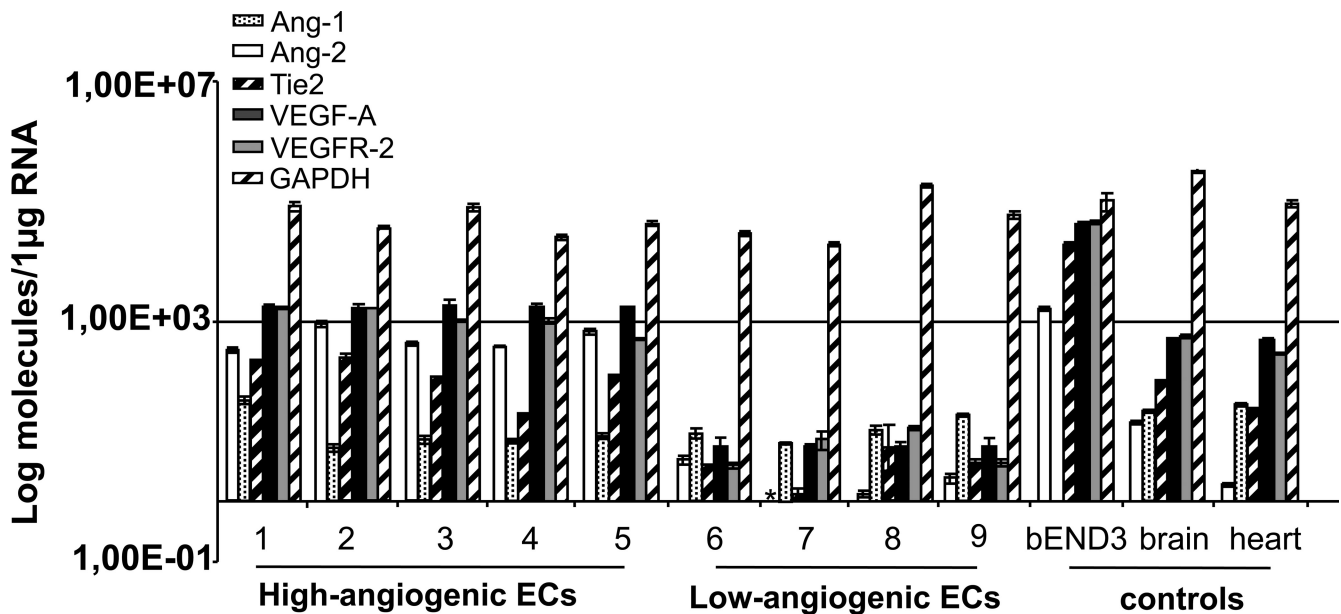
Figure 4. **Logarithmic presentation of quantitative expression analysis of angiogenic factors and corresponding receptors from micro–dissected endothelial cells of MT/ret melanoma.** Laser microdissected intratumoral endothelial cells from cryosections of high and low angiogenic-active MT/ret melanoma were used for the quantitative real-time PCR analysis of angiogenic factors and their corresponding receptors (n = 5 high and 4 low angiogenic tumors of three mice). Total RNA of bEND3 cells and mouse brain and heart was used as a control for angiogenic factor expression. The analyses for each factor were done in triplicate for each experiment. Three independently performed experiments showed corresponding outcomes. Error bars, mean ± SD.

the beginning of therapy, using fl-VCT (Fig. 5 D), and over time. In this study, PTK/ZK treatment resulted in inhibition of the development of novel tumors compared with vehicle controls (P = 0.005; Fig. 5 E) without affecting the volume of preexisting tumor at the end of therapy in both groups (Fig. 5 F). In accordance with the prevention study, immunohistological analyses revealed that the majority of preexisting tumors showed low vascular density at the end of treatment. Interestingly, PTK/ZK treatment in preexisting tumors of high angiogenic potential obviously resulted in vessel regression (Fig. S2 D), which was confirmed by detection of laminin-positive empty

vessel sleeves in the interspace between CD31-positive endothelial cells (not depicted). Immunohistochemical analyses at the end of the therapeutic PTK/ZK treatment showed, again in accordance with preventative treatment, that low vascular melanoma nodules did not respond to PTK treatment and therefore were distributed as with vehicle-treated mice (Fig. S2 D). It has been shown that bone marrow–derived cells could also contribute to the resistance to antiangiogenic therapy (Bingle et al., 2002; de Visser and Coussens, 2006). Therefore, we analyzed the recruitment of macrophages in high and low angiogenic tumors treated with vehicle or PTK/ZK during the
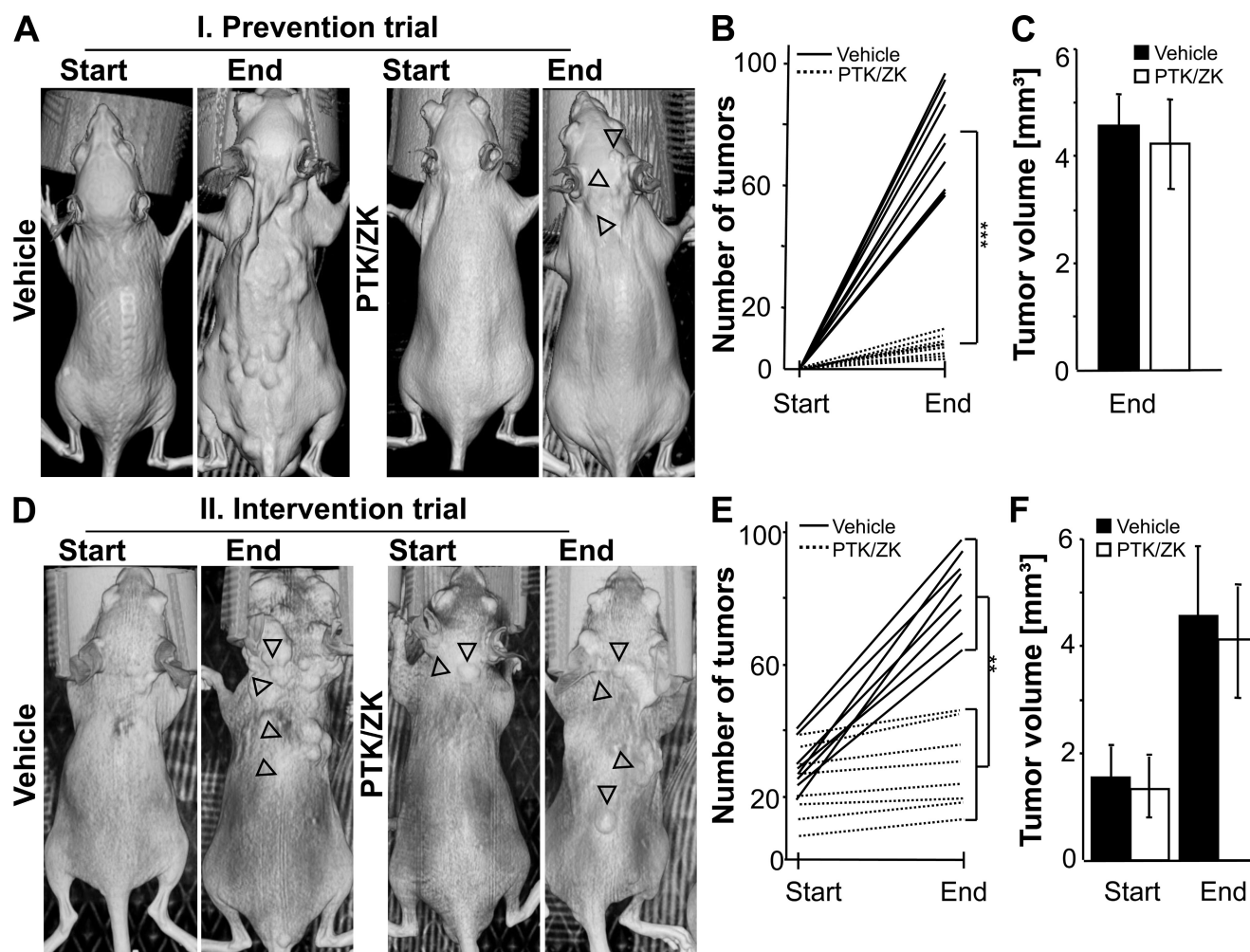
Figure 5. Analysis of prevention and therapeutic effects of PTK/ZK on melanoma development and progression in MT/*ret* transgenic mice. (A) Tumor-free mice of concordant age and sex were used for the prevention trial (*n* = 10 mice/experimental group). MT/*ret* transgenic mice, orally treated with PTK/ZK (50 mg/1 kg in 0.9% NaCl) or vehicle (0.9% NaCl) alone, were visualized at the beginning and end of therapy using fl-VCT. Therapy-resistant tumors of the PTK/ZK-treated group are highlighted by empty arrowheads. (B) Quantification of tumor development at the end of the prevention therapy in PTK/ZK-treated (*n* = 9 mice) and vehicle-treated (*n* = 10 mice) transgenic mice (***, P ≤ 0.001). (C) Total tumor volume analyses (in millimeters cubed) of vehicle-treated (*n* = 100 tumors of 10 mice) and PTK/ZK-treated (*n* = 73 tumors of nine mice) mice, grown during therapy using fl-VCT. Data of the prevention trial (A–C) were analyzed in two independently performed experiments. (D) Assessment of therapeutic effects of PTK/ZK in tumor-bearing mice screened at the beginning and end of therapy by fl-VCT (*n* = 10 mice/experimental group). Hardly observable tumors are highlighted by empty arrowheads. (E) Investigation of tumor number in vehicle- and PTK/ZK-treated mice at the beginning and at the end of therapy (*n* = 8 mice/experimental group; **, P ≤ 0.005). (F) Analyses of total tumor volume (in millimeters cubed) during the therapeutic trial using fl-VCT (*n* = 100 tumors [beginning and end] of four vehicle-treated and five PTK/ZK-treated mice). All data of intervention experiments (D–F) were independently performed twice with corresponding outcomes (*n* = 5 mice/group). Error bars, mean ± SD.

interventional setting. Immunohistological analyses for F4/80-expressing macrophages revealed that the majority was located inside the lumina of blood vessels or infiltrated as tumor cell–associated macrophages into the intratumoral areas in both tumor phenotypes without significant differences in number or localization of vehicle- or PTK/ZK-treated tumors (Fig. S3).

Mature vascular network in human melanoma metastases grown during adjuvant bevacizumab therapy

Based on our results using the murine melanoma model, we analyzed the vascular network, mural cell recruitment, and level of pericyte differentiation in human melanoma metastases, which had developed during the UK adjuvant bevacizumab trial in stage III cutaneous melanoma. In contrast to mela-noma metastases observed from patients without therapy, bevacizumab-resistant metastases displayed a 17-fold increase in the diameter of tumor-associated blood vessels (mean, 5.3 ± 2.9 vs. 83.3 ± 21.7 µm in untreated patients; $P \leq 0.001$; Fig. 6 A), as well as an eightfold increase (mean, 305.3 ± 39.8 vs. 68.9 ± 23.0 µm) in vessel perimeter ($P \leq 0.001$; Fig. 6 B). Interestingly, all blood vessels of bevacizumab-resistant tumors, identified by expression of CD31 (Fig. 6 C), exhibited mature vessel morphology by the expression of the early differentiation marker Desmin (not depicted) and the late marker α-SMA (Fig. 6 E) in contrast to the majority of blood vessels of metastases from patients without bevacizumab therapy, where detection of desmin and α-SMA–covered blood vessels could not be observed (Fig. 6, D and F).
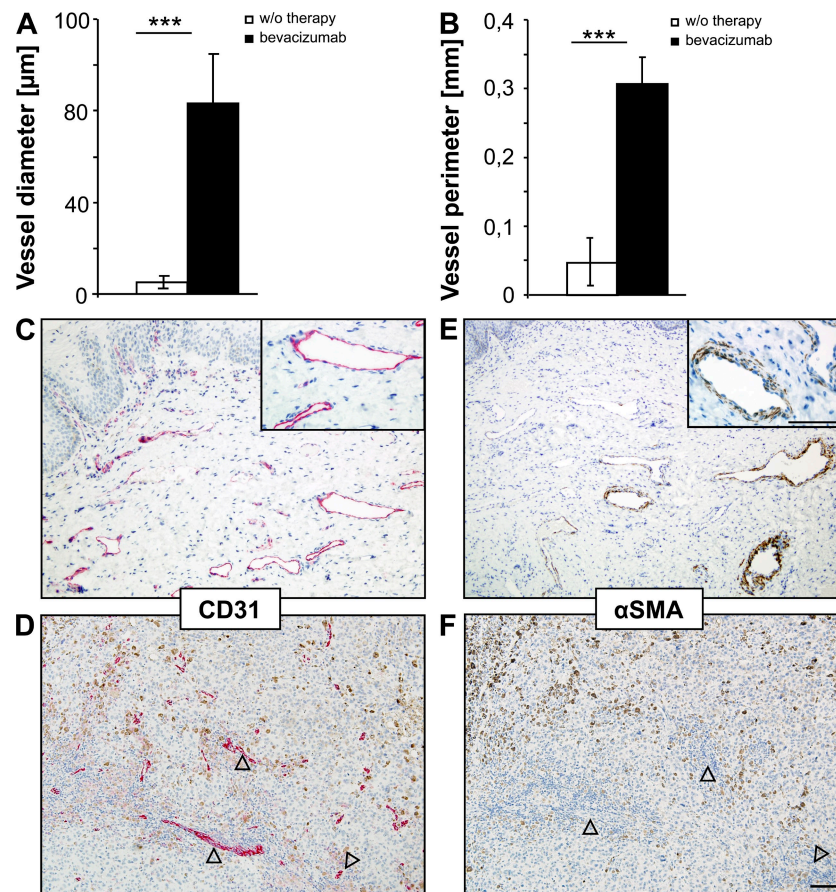
Figure 6. Immunohistological and morphometric analyses of the vascular network in bevacizumab–resistant human melanoma metastases. (A and B) Quantification for vessel diameter (in micrometers; A) or vessel perimeter (in millimeters; B) of all existent tumor-associated blood vessels in melanoma metastases of patients receiving bevacizumab therapy ($n = 100$ vessels in three metastases of three patients), compared with metastases, isolated from patients without therapy ($n = 100$ vessels in 10 tumors of 10 patients; ***, $P \leq 0.001$). (C and D) Immunohistochemical detection of blood vessels using the endothelial cell marker CD31 (red) in cutaneous bevacizumab-resistant metastases (C) versus melanoma metastases developed off therapy (D). Arrowheads indicate tumor-associated blood vessels for better visualization. (E and F) Analysis of mural cell recruitment using the late stage differentiation marker α-SMA (brown) in therapy-resistant melanoma (E) and cutaneous metastases developed in patients without treatment (F). Arrowheads indicate the blood vessel location of the corresponding tumor section used for CD31 detection (D). Nuclei were counterstained using Hematoxylin. All immunohistochemical analyses (C–F) were done using all available and existent melanoma metastases ($n = 3$ metastases of three patients) of patients receiving bevacizumab therapy or melanoma metastases ($n = 10$ metastases of 10 patients) of patients without therapy. Immunohistological detection was performed twice with concordant results. Representative images of analyzed melanoma metastases are presented in C and D. Error bars, mean ± SD. Bars, 100 µm.

DISCUSSION

In our study, we analyzed human melanoma metastases taken at clinical relapse in patients undergoing adjuvant treatment with bevacizumab (Avastin[R]), but we also analyzed a corresponding murine model in which melanomas develop spontaneously. In both systems, tumor development during anti–VEGF therapy (bevacizumab in humans and PTK/ZK in mice) was characterized by a mature intratumoral vascular network and stabilization of the vascular wall. The level of mural cell differentiation for vessel maturation and the process of vessel stabilization by pericyte coverage are believed to be major mediators for priming blood vessels to its sensitivity to anti-VEGF therapy.

We also present, for the first time, a murine model (MT/*ret*) developing spontaneously metastasizing melanoma characterized by high, but also low, angiogenic-active tumors in parallel. This vascular phenotype is independent of tumor volume or location. Fast growing highly angiogenic-active tumors exhibit hypoxia-driven Ang-2 expression, leading to immature intratumoral vascular network, basal lamina defects, and loss of pericytes. In contrast, low angiogenic-active tumor nodules displayed stabilized vessels, a slower growth kinetic, and increased vessel lumina. Highly vascularized tumors were characterized by significant tumor regression in the adjuvant and remodelling of the tumor vascular bed in the advanced therapy setting. Interestingly, low angiogenic-active tumors did not respond to anti-VEGF therapy using the small-molecule inhibitor PTK/ZK. Careful expression profiling analysis of laser microdissected tumor-associated endothelial cells from both vascular beds revealed a significant decrease in expression of proangiogenic factors Ang-2 and VEGF-A and their receptors Tie2 and VEGFR-2 in VEGF-resistant MT/*ret* tumors. In summary, the most prominent differences between the two vascular beds observed in this melanoma model were the vessel structure (vessel density, vessel diameter/perimeter distribution, level of mural cell differentiation, and pericyte coverage or basement membrane investment) and the expression profile of the vascular-specific receptor tyrosine kinase systems.

The concept of antiangiogenic cancer therapy seems simple at the first look; destroying tumor vasculature and depriving the tumor of nutrients and oxygen will ultimately induce tumor regression. The long-term survival benefit in patients of targeting the VEGF signaling pathway has not been so affirmative as initially hoped and better clinical outcomes have been seen in combination with chemotherapy (Hurwitz et al., 2004) or additional drugs (Perez et al., 2009). A key finding in this context is that VEGF-A/VEGFR-2 blockage leads transiently to vessel remodeling and normalization of the tumor vascular bed, as described by increased pericyte coverage of tumor vessels. This results in vessel stabilization and reduced vascular permeability, which facilitates access of coadministered chemotherapeutic drugs (Jain 2005).

The role of VEGF in pericyte biology is less clear, and experiments aimed at specifically addressing the role of pericytes in responses to antiangiogenic cancer therapies are rare

or lacking. Consequently, such experiments will need to be performed in genetically manipulated models, resembling the human situation in aspects of tumor development and angiogenesis. Conventional mouse melanoma models (e.g., B16), based on the transplantation of tumor cells, are not suitable for such studies. Transplantation of tumor cells triggers infiltration of immune cells such as macrophages, which are known to mediate important processes during tumor angiogenesis (Hagemann et al., 2009; Shieh et al., 2009), and the natural situation of tumor development and histology of the disease is not comparable with the clinical situation. Now, based on our findings, the MT/*ret* transgenic mouse model is the first model which fulfills all criteria of endogenously driven spontaneous tumor development and angiogenesis and presents, for the first time, VEGF-dependent and –independent tumor growth in parallel. Interestingly, distribution of both vascular beds does not correlate with tumor volume or location. In addition, there was not an experimental hint that low angiogenic tumors engage an angiogenic switch during progression and metastasis leading to neovascularization and vessel destabilization.

The observed altered pattern of mural cell recruitment into the vascular wall and the maturation of blood vessels in both vascular phenotypes, and their role for susceptibility to antiangiogenic therapy, was our most surprising finding. However, the mechanisms of Ang–induced mural cell recruitment have not been elucidated. Mechanistically, the most well understood pathway of endothelial cell–directed mural cell recruitment is through paracrine-acting PDGF-B (Abramsson et al., 2003). However, the molecular cross talk between the Ang–Tie and PDGF–PDGFR systems has not yet been resolved. In previous studies, we were able to show that host-derived Ang-2 is able to affect early stages of tumor development and vessel maturation (Nasarre et al., 2009). Thus, our data suggest that hypoxia-triggered up-regulation of Ang-2, detected by laser microdissection of tumor-associated endothelial cells of high angiogenic melanoma, resulted in vessel destabilization by loss of pericyte coverage, followed by induction of neovascularization. This corresponds with recent in vitro observations of hypoxia-regulated Ang-2 expression in endothelial cells (Pichiule et al., 2004). These data confirm our recent finding that Ang-2 expression levels correlate with disease progression and metastasis in sera of melanoma patients (Helfrich et al., 2009) and suggests again that the Ang–Tie system might have a more direct effect on mural cell recruitment and maturation than previously thought. Interestingly, differences in the expression of Ang-1 could not be observed between vascular phenotypes. Ang-1 and Ang-2 have been described to exert opposing functions during vessel development. Although Ang-1–induced Tie2 activation transduces survival signals and leads to vessel stabilization and maturation (Suri et al., 1996), Ang-2 acts as a vessel destabilizing agent that induces permeability and leads to dissociation of cell–cell contacts in cultured endothelial cells (Scharpfenecker et al., 2005). This leads to the speculation that if Ang-2 as an antagonistic Tie2 ligand has a stronger binding capacity for the

induction of Tie2 activation compared with Ang-1, resulting in mural cell depletion and vessel destabilization independent of the presence of Ang-1 expression.

Among the most surprising findings of the present study was the altered pattern of mural cell recruitment and maturation of blood vessels in human melanoma metastases taken at clinical relapse in patients undergoing adjuvant anti-VEGF therapy using bevacizumab. These observations were paralleled by our corresponding melanoma model using PTK/ZK. In both experimental settings tumor vessels, which are resistant to anti–VEGF therapy, were characterized by increased vessel diameter, normalization of the vascular bed by coverage of mature pericytes, and immunoreactivity for Desmin, NG-2, PDGFR-β, and the late stage maturity marker α-SMA. Based on the finding that PTK/ZK–resistant blood vessels of MT/*ret* transgenic tumors showed only minor expression of proangiogenic factors (e.g., Ang-2 and VEGF-A), resulting in low angiogenic potential and resistance to the traditional antiangiogenic approaches, it is highly desirable to identify alternative ways to modulate tumor vasculature that do not interfere with the complex regulatory network of proangiogenic factors.

Our findings demonstrate the role of mural cell recruitment and maturation for the susceptibility to anti-VEGF cancer therapy. The findings warrant further mechanistic analysis to focus on the molecular cross talk between Ang/Tie and PDFG/PDGFR signaling during mural cell recruitment and maturation. This may contribute to a more rational therapeutic exploitation of antiangiogenic therapy approaches. In this context, it would be of considerable interest to analyze biopsies from patients whose tumors are progressive despite VEGF/VEGFRs blockage. Results of such studies would lead to clinical studies trying to combine modalities targeting tumor angiogenesis by inhibition of VEGF signaling and blockage of mural cell recruitment, as well as maturity by inhibition of PDGF–B pathways. Future work using combination therapies targeting the implicated pathways and analyses of maturation kinetics in spontaneous mouse models will pave the way to the rational development of a second generation of antiangiogenic combination therapies to overcome the problem of therapy resistance.

MATERIALS AND METHODS

Mice. Mice (C57BL/6) expressing the human *ret* proto-oncogene under the control of the mouse metallothionein I promoter-enhancer (Kato et al., 1998) were provided by M. Kato (Chubu University, Aichi, Japan). MT/*ret* transgenic mice develop spontaneously cutaneous malignant melanoma metastasizing to lymph nodes, spleen, lung, and brain that resemble human melanoma in many aspects of histopathology and clinical development (Kato et al., 1998). Mice were crossed with C57BL/6 wild-type mice for heterozygous transgene expression and kept under specific pathogen-free conditions in the animal facility of the German Cancer Research Center (Heidelberg, Germany) and the Central Animal Laboratory at the University Hospital Essen (Essen, Germany). Experiments were performed in accordance with government and institute guidelines and regulations. For definition of tumor development, mice were monitored for indicated time points using fl-VCT (Siemens). Animal procedures were approved by the Regierungspräsidium, Karlsruhe, and the Landesamt für Natur, Umwelt und Verbraucherschutz Nordrhein-Westfalen, Germany.

Human tumor samples. Melanoma metastases of 59–66-yr-old patients, developed between 2 and 8 wk after receiving 8–11 cycles of bevacizumab (Avastin[R]) as adjuvant therapy after resection of AJCC stage IIB, IIC, and III cutaneous melanoma, and metastases of patients off therapy (concordant age and gender) were assessed for their vascular bed and vessel maturity by immunohistochemistry. All available biopsies from patients relapsing on the treatment arm of the randomized-controlled clinical phase III study AVAST-M (adjuvant aVAStin trial in high-risk melanoma), evaluating the VEGF inhibitor bevacizumab, were obtained from October 2008 onward. Informed patient consent and the appropriate Institutional Review Board approval was obtained for all patients and relapses were confirmed by histological examination. Human protocols were approved by the Oxford Research Ethics Committee C (reference 07/H0606/112, tissue banking) and the trial approval for AVAST-M (07/Q1606/15).

Immunohistochemistry. Consecutive cryosections (MT/*ret* melanoma) and paraformaldehyde-fixed paraffin sections (human melanoma metastases) were processed for immunostaining. For detection of the endothelial cell marker CD31, cryosections were fixed with acetone/methanol (1:1) and endogenous peroxidase was blocked with 3% H_2O_2, followed by avidin/biotin blocking. Nonspecific binding was blocked with 5% rabbit serum/1% bovine serum albumin in PBS + 0.02% Tween for 30 min. Rat anti–mouse PECAM-1 (BD), sheep anti–human PECAM-1 (R&D Systems), or ChromPure goat IgG (Dianova), used as negative control, were incubated and visualized using DAB or AEC Substrate Chromogen system (Dako), followed by counterstaining of nuclei using Meyer's Hemalaun solution (Merck). For the visualization of endothelial–pericyte association in MT/*ret* tumors, double stainings were performed using rat anti-CD31 (PECAM-1; BD) combined with rabbit anti-Desmin antibody (Abcam), rabbit anti-NG2 (Millipore), rat anti-CD140b (PDGFR-β; eBioscience), or mouse anti–α-SMA direct-labeled Cy3 antibody (Sigma-Aldrich). Mural cells in human metastases were detected using mouse anti–α-SMA (Sigma-Aldrich) and mouse anti-Desmin antibody (Dako). Cell proliferation was assessed by immunostaining with rat anti–Ki-67 antibody (clone TEC-3; Dako), basal lamina was visualized by rabbit anti-laminin (Sigma-Aldrich), and lymphatic endothelial cells were assessed using rabbit anti–Lyve-1 (ReliaTech), all of which were counterstained with PECAM-1 for vessel detection. Macrophage recruitment was analyzed using rat anti-F4/80 antigen (AbD Serotec). The number of macrophages was calculated as F4/80-expressing macrophages per tumor area (in millimeters squared) using microscopes (Olympus) and corresponding Cell P Software (Olympus). For the detection of expression of the melanogenic enzymes tyrosinase, TRP-1, and gp-100, paraffin-embedded tumor sections of 8 μm were deparaffinized, followed by antigen retrieval using 1 mM EDTA at 90°C for 10 min, blocking of nonspecific bindings, and incubation of primary antibodies over night at 4°C. Antibodies against tyrosinase, TRP-1, and gp-100 were provided by V. Hearing (National Institutes of Health, Bethesda, MD). Lymph endothelial cells were detected using rabbit anti–Lyve-1 antibody (ReliaTech). Apoptotic cells were detected by the MEBSTAIN Apoptosis Kit II (MBL International) and quantified as percentage of TUNEL-positive areas per field. Primary antibodies were detected by rabbit anti–rat Alexa Fluor 594, rabbit anti–rat Alexa Fluor 488, or donkey anti–rabbit Alexa Fluor 594 (all from Invitrogen). Nuclei were counterstained using propidium iodide. Slide fluorescence was examined by confocal laser-scanning microscopy (TCS SP2; Leica).

Hypoxic tumor areas were detected by the formation of pimonidazole adducts after injection of pimonidazole hydrochloride compound into tumor-bearing animals for 30 min. Tumor sections were immunostained using the Hypoxyprobe-1 Plus kit according to the manufacturer's protocol (Natural Pharmacia International, Inc.). The hypoxic area index was quantified as the percentage of positive tumor area per total tumor area in tumors of corresponding volume.

Morphometric analysis of tumor vessels and pericyte coverage. Morphogenic analyses of MT/ret tumors were done using consecutive cryosections stained for the endothelial cell marker CD31. The quantification of MVD and corresponding tumor volume was calculated using the mean of

three tumor sections per tumor (top, middle, and base) of concordant distance. MVD was calculated as number of vessels per tumor area. Intratumoral vessel perimeter and vessel–vessel distance were measured in tumors of high and low vessel density. The percentage of high angiogenic or low vascularized tumors per mouse was analyzed by isolation of all tumors per mouse followed by endothelial cell detection using immunohistochemistry. Pericyte coverage was assessed using the pericyte marker NG-2, Desmin, PDGFR-β, or α-SMA in combination with CD31 for the detection of individual phases during pericyte differentiation. All vessels per tumor were counted using multiple alignment function. For the assessment of pericyte coverage in human melanoma metastases, paraffin sections of all available bevacizumab-resistant cutaneous metastases and metastases developing off therapy were costained for the endothelial cell marker CD31 and pericyte markers as described for murine analyses. All present vessels were analyzed for vessel perimeter and diameter as described earlier in this section. All morphometric analyses were performed on Olympus microscopes and corresponding Cell P Software.

Assessment of vessel perfusion and stability. Tumor-bearing MT/ret transgenic mice were injected through the tail vein 20 min before killing by cervical dislocation using 150 μg FITC-conjugated lectin/150 μl 0.9% NaCl from *Bandeiraea simplicifolia* (Sigma-Aldrich). A perfusion index was quantified as the percentage of lectin-positive per CD31-positive vessels in high and low angiogenic-active tumors. For assessment of vascular stability, mice were injected via tail vein using 1 mg/100 μl FITC-conjugated dextran (3.000 mol wt). After 15 min of incubation, mice were killed and histological analyses were performed.

Laser microdissection of tumor-associated endothelial cells. 10-μm cryosections of murine melanoma were cut under RNase-free conditions, fixed with 70% ethanol in DEPC, and stained for the identification of tumor morphology using Meyer's Hemalaun solution for 1 min and EosinY for 1 s (both Merck). Intratumoral endothelial cells were isolated from five high and four low angiogenic tumors using the P.A.L.M. MicroBeam Microscope (Carl Zeiss, Inc.). RNA of microdissected endothelial cells was isolated using the RNeasy micro kit (QIAGEN) according to the manufacturer's instructions. Expression analysis of dissected tumor-associated endothelial cells was done by quantitative real-time PCR using 1 μg of total cellular RNA for reverse transcription.

Quantitative real-time PCR. Specific primers of angiogenic factors and their receptors were designed to detect the amounts of various messenger RNA species in tumor-associated endothelial cells of the high angiogenic-active as well as low vascularized melanomas. For the generation of the standard, each primer pair was subjected to an endpoint PCR in a final volume of 30 μl using 1 μl bEND3 complementary DNA (cDNA; for Ang-2, Tie2, VEGF, and VEGFR) or BALB/c fibroblast cDNA (for Ang-1) with 0.2 U Taq polymerase (GeneCraft), 500 nM dNTP, 3 μl 10× buffer (provided by Bio-Rad Laboratories), and 0.5 μM of the particular sense and antisense primers under standard conditions (at 95°C for 3 min followed by 34 cycles at 95°C for 30 s, 60°C for 45 s, and 72°C for 30 s and an extention at 72°C for 8 min). Afterward, the PCR product was purified with PCR purification kit and cloned in the pDrive cloning vector with the PCR cloning kit (both QIAGEN). Colonies were determined for presence of the insert and the DNA was subsequently sequenced. Finally, 1 μl each of cDNA or standard DNA within the range of 10^3 to 10^8 molecules was amplified with SYBR green master mix (Bio-Rad Laboratories) and primers in a final volume of 25 μl according to the manufacturer's protocol. The total RNA of bEnd3 cells, a mouse endothelial cell line derived from cortex blood vessels and mouse heart and brain was isolated using the RNeasy kit (QIAGEN). Afterward, 1 μg of each sample was reverse transcribed with the QuantiTect Reverse Transcription kit in a final volume of 20 μl (QIAGEN). The following primers were used: *mGAPDH* forward, 5′-TGACCACAGTC-CATGCCCATA-3′, and reverse, 5′-GACGGACACATTGGGGGTAG-3′; *mVEGF-A* forward, 5′-ACTGGACCCTGGCTTTACTG-3′, and reverse,

5′-ACACAGGACGGCTTGAAGAT-3′; *mVEGFR2* forward, 5′-TTCT-GGACTCTCCCTGCCTA-3′, and reverse, 5′-TCTGTCTGGCTGTC-ATCTGG-3′; *mAng-1* forward, 5′-AGGCTTGGTTTCTCGTCAGA-3′, and reverse, 5′-TCTGCACAGTCTCGAAATGG-3′; *mAng-2* forward, 5′-CACAGCGAGCAGCTACAGTC-3′, and reverse, 5′-ATAGCAACC-GAGCTCTTGGA-3′; and *mTie2* forward, 5′-TCTGGGTGGCCAC-TACCTAC-3′, and reverse 5′- TGAAAGGCTTTTCCACCATC-3′.

Electron microscopy. Electron microscopy was used for the assessment of ultrastructural analyses of intratumoral vessels. Tumor samples were isolated and divided in half. One half was used for electron microscopy and fixed in 2.5% glutaraldehyde in 0.1 M cacodylate buffer. The corresponding half was used for identification of tumor vascularization by immunohistochemistry. Semithin sections from glutaraldehyde-fixed epoxy resin–embedded specimens were stained with paraphenylen diamine for light microscopy (Weis and Schröder, 1989). Ultrathin sections of osmium-treated tissue were contrast enhanced with lead citrate and uranyl acetate for electron microscopy (Weis et al., 1995). The ultrastructure of tumor vessels of both vascular phenotypes was studied in ultrathin sections using an electron microscope (902; Carl Zeiss, Inc.) equipped with a digital camera. On each section, five to six tissue areas were analyzed and used for semiquantitative assessment of vessel phenotype in each tumor group.

fl-VCT. For the evaluation of tumor number and volume in the MT/*ret* transgenic mouse line, mice scanning was performed under inhalation narcosis, using an fl-VCT scanner (Siemens) at the indicated time points (Kiessling et al., 2004; Gupta et al., 2006). Total scan time was 40 s with a rotation time of 21 s. A tube voltage of 80 kV and a tube current of 50 mA with continuous radiation were selected. The reconstruction field of view was 4.5 cm transaxially with a reconstruction matrix of 512 × 512 pixels and an axial slice spacing of 0.2 mm resulting in a voxel size of $0.08 \times 0.08 \times 0.2$ mm^3. A modestly sharp reconstruction kernel (H80s) was used for image reconstruction. Image postprocessing was performed using standard three-dimensional postprocessing steps, for example, volume rendering. The reconstructed volume datasets were fitted with a standard DICOM header and transferred to a standard radiological postprocessing workstation. The amount of metastasis was counted by reviewing the datasets on multiplanar reformations. Standard size measurement software was used for the quantification of tumor number and volume (InSpace; Siemens). For tumor volume calculation, two orthogonal tumor diameters were taken using the virtual caliper tool.

Antiangiogenic treatment using PTK/ZK. MT/*ret* transgenic mice (concordant age and sex per group) were monitored by fl-VCT for the individual status of tumor development. Mice were treated at 2 wk of age (prevention, tumor free) or at 4 wk (therapeutic intervention, tumor bearing) by oral administration of PTK/ZK (Novartis; 50 mg/kg dissolved in 0.9% NaCl) or vehicle (0.9% NaCl) alone, as a control, twice a day over a period of 4 wk. Mice were measured at the beginning, weekly during treatment, and at the end of therapy for assessment of tumor number and volume. At the end of therapy, tumors were isolated and analyzed by immunohistochemistry. Experimental series (intervention and prevention) were repeated twice.

Statistical analysis. Student's *t* test was used for the determination of statistical significance between experimental groups. All results were expressed as mean ± SD. P-values <0.05 were considered statistically significant.

Online supplemental material. Fig. S1 shows the characterization of the MT7ret mouse model. Fig. S2 analyzes the effects of PTK/ZK on vessel formation in melanoma of MT/ret transgenic mice. Fig. S3 displays the effects of PTK/ZK on macrophage recruitment in high and low angiogenic tumors of MT/ret melanoma. Online supplemental material is available at http://www.jem.org/cgi/content/full/jem.20091846/DC1.

REFERENCES

Abramsson, A., P. Lindblom, and C. Betsholtz. 2003. Endothelial and nonendothelial sources of PDGF-B regulate pericyte recruitment and influence vascular pattern formation in tumors. *J. Clin. Invest.* 112:1142–1151.

Andrae, J., R. Gallini, and C. Betsholtz. 2008. Role of platelet-derived growth factors in physiology and medicine. *Genes Dev.* 22:1276–1312. doi:10.1101/gad.1653708

Armulik, A., A. Abramsson, and C. Betsholtz. 2005. Endothelial/pericyte interactions. *Circ. Res.* 97:512–523. doi:10.1161/01.RES.0000182903.16652.d7

Benjamin, L.E., I. Hemo, and E. Keshet. 1998. A plasticity window for blood vessel remodelling is defined by pericyte coverage of the preformed endothelial network and is regulated by PDGF-B and VEGF. *Development.* 125:1591–1598.

Bergers, G., S. Song, N. Meyer-Morse, E. Bergsland, and D. Hanahan. 2003. Benefits of targeting both pericytes and endothelial cells in the tumor vasculature with kinase inhibitors. *J. Clin. Invest.* 111:1287–1295.

Betsholtz, C., P. Lindblom, and H. Gerhardt. 2005. Role of pericytes in vascular morphogenesis. *EXS.* 94:115–125.

Bingle, L., N.J. Brown, and C.E. Lewis. 2002. The role of tumour-associated macrophages in tumour progression: implications for new anticancer therapies. *J. Pathol.* 196:254–265. doi:10.1002/path.1027

Carlson, T.R., Y. Feng, P.C. Maisonpierre, M. Mrksich, and A.O. Morla. 2001. Direct cell adhesion to the angiopoietins mediated by integrins. *J. Biol. Chem.* 276:26516–26525. doi:10.1074/jbc.M100282200

Carmeliet, P. 2005. Angiogenesis in life, disease and medicine. *Nature.* 438:932–936. doi:10.1038/nature04478

de Visser, K.E., and L.M. Coussens. 2006. The inflammatory tumor microenvironment and its impact on cancer development. *Contrib. Microbiol.* 13:118–137. doi:10.1159/000092969

Döme, B., S. Paku, B. Somlai, and J. Tímár. 2002. Vascularization of cutaneous melanoma involves vessel co-option and has clinical significance. *J. Pathol.* 197:355–362. doi:10.1002/path.1124

Erber, R., A. Thurnher, A.D. Katsen, G. Groth, H. Kerger, H.P. Hammes, M.D. Menger, A. Ullrich, and P. Vajkoczy. 2004. Combined inhibition of VEGF and PDGF signaling enforces tumor vessel regression by interfering with pericyte-mediated endothelial cell survival mechanisms. *FASEB J.* 18:338–340.

Escudier, B., T. Eisen, W.M. Stadler, C. Szczylik, S. Oudard, M. Siebels, S. Negrier, C. Chevreau, E. Solska, A.A. Desai, et al; TARGET Study Group. 2007. Sorafenib in advanced clear-cell renal-cell carcinoma. *N. Engl. J. Med.* 356:125–134. doi:10.1056/NEJMoa060655

Fallowfield, M.E., and M.G. Cook. 1991. The vascularity of primary cutaneous melanoma. *J. Pathol.* 164:241–244. doi:10.1002/path.1711640309

Ferrara, N., and R.S. Kerbel. 2005. Angiogenesis as a therapeutic target. *Nature.* 438:967–974. doi:10.1038/nature04483

Ferrara, N., K.J. Hillan, H.P. Gerber, and W. Novotny. 2004. Discovery and development of bevacizumab, an anti-VEGF antibody for treating cancer. *Nat. Rev. Drug Discov.* 3:391–400. doi:10.1038/nrd1381

Fiedler, U., and H.G. Augustin. 2006. Angiopoietins: a link between angiogenesis and inflammation. *Trends Immunol.* 27:552–558. doi:10.1016/j.it.2006.10.004

Fiedler, U., M. Scharfenecker, S. Koidl, A. Hegen, V. Grunow, J.M. Schmidt, W. Kriz, G. Thurston, and H.G. Augustin. 2004. The Tie-2 ligand angiopoietin-2 is stored in and rapidly released upon stimulation from endothelial cell Weibel-Palade bodies. *Blood.* 103:4150–4156. doi:10.1182/blood-2003-10-3685

Folkman, J., K. Watson, D. Ingber, and D. Hanahan. 1989. Induction of angiogenesis during the transition from hyperplasia to neoplasia. *Nature.* 339:58–61. doi:10.1038/339058a0

Gerhardt, H., and C. Betsholtz. 2003. Endothelial-pericyte interactions in angiogenesis. *Cell Tissue Res.* 314:15–23. doi:10.1007/s00441-003-0745-x

Gupta, R., M. Grasruck, C. Suess, S.H. Bartling, B. Schmidt, K. Stierstorfer, S. Popescu, T. Brady, and T. Flohr. 2006. Ultra-high resolution flat-panel volume CT: fundamental principles, design architecture, and system characterization. *Eur. Radiol.* 16:1191–1205. doi:10.1007/s00330-006-0156-y

Hagemann, T., S.K. Biswas, T. Lawrence, A. Sica, and C.E. Lewis. 2009. Regulation of macrophage function in tumors: the multifaceted role of NF-kappaB. *Blood.* 113:3139–3146. doi:10.1182/blood-2008-12-172825

Hanahan, D. 1997. Signaling vascular morphogenesis and maintenance. *Science.* 277:48–50. doi:10.1126/science.277.5322.48

Hanahan, D., and J. Folkman. 1996. Patterns and emerging mechanisms of the angiogenic switch during tumorigenesis. *Cell.* 86:353–364. doi:10.1016/S0092-8674(00)80108-7

Helfrich, I., L. Edler, A. Sucker, M. Thomas, S. Christian, D. Schadendorf, and H.G. Augustin. 2009. Angiopoietin-2 levels are associated with disease progression in metastatic malignant melanoma. *Clin. Cancer Res.* 15:1384–1392. doi:10.1158/1078-0432.CCR-08-1615

Hellström, M., M. Kalén, P. Lindahl, A. Abramsson, and C. Betsholtz. 1999. Role of PDGF-B and PDGFR-beta in recruitment of vascular smooth muscle cells and pericytes during embryonic blood vessel formation in the mouse. *Development.* 126:3047–3055.

Hess-Stumpp, H., M. Haberey, and K.H. Thierauch. 2005. PTK 787/ZK 222584, a tyrosine kinase inhibitor of all known VEGF receptors, represses tumor growth with high efficacy. *ChemBioChem.* 6:550–557. doi:10.1002/cbic.200400305

Holash, J., P.C. Maisonpierre, D. Compton, P. Boland, C.R. Alexander, D. Zagzag, G.D. Yancopoulos, and S.J. Wiegand. 1999. Vessel cooption, regression, and growth in tumors mediated by angiopoietins and VEGF. *Science.* 284:1994–1998. doi:10.1126/science.284.5422.1994

Hurwitz, H., L. Fehrenbacher, W. Novotny, T. Cartwright, J. Hainsworth, W. Heim, J. Berlin, A. Baron, S. Griffing, E. Holmgren, et al. 2004. Bevacizumab plus irinotecan, fluorouracil, and leucovorin for metastatic colorectal cancer. *N. Engl. J. Med.* 350:2335–2342. doi:10.1056/NEJMoa032691

Ilmonen, S., A.L. Kariniemi, T. Vlaykova, T. Muhonen, S. Pyrhönen, and S. Asko-Seljavaara. 1999. Prognostic value of tumour vascularity in primary melanoma. *Melanoma Res.* 9:273–278.

Jain, R.K. 2005. Normalization of tumor vasculature: an emerging concept in antiangiogenic therapy. *Science.* 307:58–62. doi:10.1126/science.1104819

Kato, M., M. Takahashi, A.A. Akhand, W. Liu, Y. Dai, S. Shimizu, T. Iwamoto, H. Suzuki, and I. Nakashima. 1998. Transgenic mouse model for skin malignant melanoma. *Oncogene.* 17:1885–1888. doi:10.1038/sj.onc.1202077

Kiessling, F., S. Greschus, M.P. Lichy, M. Bock, C. Fink, S. Vosseler, J. Moll, M.M. Mueller, N.E. Fusenig, H. Traupe, and W. Semmler. 2004. Volumetric computed tomography (VCT): a new technology for non-invasive, high-resolution monitoring of tumor angiogenesis. *Nat. Med.* 10:1133–1138. doi:10.1038/nm1101

Kunkel, P., S. Müller, P. Schirmacher, D. Stavrou, R. Fillbrandt, M. Westphal, and K. Lamszus. 2001. Expression and localization of scatter factor/hepatocyte growth factor in human astrocytomas. *Neuro-oncol.* 3:82–88. doi:10.1215/15228517-3-2-82

Küsters, B., W.P. Leenders, P. Wesseling, D. Smits, K. Verrijp, D.J. Ruiter, J.P. Peters, A.J. van Der Kogel, and R.M. de Waal. 2002. Vascular endothelial growth factor-A(165) induces progression of melanoma brain metastases without induction of sprouting angiogenesis. *Cancer Res.* 62:341–345.

Leenders, W., N. Lubsen, M. van Altena, M. Clauss, M. Deckers, C. Löwik, G. Breier, D. Ruiter, and R. de Waal. 2002. Design of a variant of vascular endothelial growth factor-A (VEGF-A) antagonizing KDR/Flk-1 and Flt-1. *Lab. Invest.* 82:473–481.

Leenders, W.P., B. Küsters, and R.M. de Waal. 2002. Vessel co-option: how tumors obtain blood supply in the absence of sprouting angiogenesis. *Endothelium.* 9:83–87. doi:10.1080/10623320212006

Maisonpierre, P.C., C. Suri, P.F. Jones, S. Bartunkova, S.J. Wiegand, C. Radziejewski, D. Compton, J. McClain, T.H. Aldrich, N. Papadopoulos, et al. 1997. Angiopoietin-2, a natural antagonist for Tie2 that disrupts in vivo angiogenesis. *Science*. 277:55–60. doi:10.1126/science.277.5322.55

Morikawa, S., P. Baluk, T. Kaidoh, A. Haskell, R.K. Jain, and D.M. McDonald. 2002. Abnormalities in pericytes on blood vessels and endothelial sprouts in tumors. *Am. J. Pathol*. 160:985–1000.

Nasarre, P., M. Thomas, K. Kruse, I. Helfrich, V. Wolter, C. Deppermann, D. Schadendorf, G. Thurston, U. Fiedler, and H.G. Augustin. 2009. Host-derived angiopoietin-2 affects early stages of tumor development and vessel maturation but is dispensable for later stages of tumor growth. *Cancer Res*. 69:1324–1333. doi:10.1158/0008-5472.CAN-08-3030

Nehls, V., K. Denzer, and D. Drenckhahn. 1992. Pericyte involvement in capillary sprouting during angiogenesis in situ. *Cell Tissue Res*. 270:469–474. doi:10.1007/BF00645048

Neufeld, G., T. Cohen, S. Gengrinovitch, and Z. Poltorak. 1999. Vascular endothelial growth factor (VEGF) and its receptors. *FASEB J*. 13:9–22.

Paku, S. 1998. Current concepts of tumor-induced angiogenesis. *Pathol. Oncol. Res*. 4:62–75. doi:10.1007/BF02904699

Perez, D.G., V.J. Suman, T.R. Fitch, T. Amatruda III, R.F. Morton, S.Z. Jilani, C.L. Constantinou, J.R. Egner, L.A. Kottschade, and S.N. Markovic. 2009. Phase 2 trial of carboplatin, weekly paclitaxel, and bi-weekly bevacizumab in patients with unresectable stage IV melanoma: a North Central Cancer Treatment Group study, N047A. *Cancer*. 115:119–127. doi:10.1002/cncr.23987

Pezzella, F., U. Pastorino, E. Tagliabue, S. Andreola, G. Sozzi, G. Gasparini, S. Menard, K.C. Gatter, A.L. Harris, S. Fox, et al. 1997. Non-small-cell lung carcinoma tumor growth without morphological evidence of neo-angiogenesis. *Am. J. Pathol*. 151:1417–1423.

Pichiule, P., J.C. Chavez, and J.C. LaManna. 2004. Hypoxic regulation of angiopoietin-2 expression in endothelial cells. *J. Biol. Chem*. 279:12171–12180. doi:10.1074/jbc.M305146200

Scharpfenecker, M., U. Fiedler, Y. Reiss, and H.G. Augustin. 2005. The Tie-2 ligand angiopoietin-2 destabilizes quiescent endothelium through an internal autocrine loop mechanism. *J. Cell Sci*. 118:771–780. doi:10.1242/jcs.01653

Shieh, Y.S., Y.J. Hung, C.B. Hsieh, J.S. Chen, K.C. Chou, and S.Y. Liu. 2009. Tumor-associated macrophage correlated with angiogenesis and progression of mucoepidermoid carcinoma of salivary glands. *Ann. Surg. Oncol*. 16:751–760. doi:10.1245/s10434-008-0259-6

Siemeister, G., M. Schirner, P. Reusch, B. Barleon, D. Marmé, and G. Martiny-Baron. 1998. An antagonistic vascular endothelial growth factor (VEGF) variant inhibits VEGF-stimulated receptor autophosphory-lation and proliferation of human endothelial cells. *Proc. Natl. Acad. Sci. USA*. 95:4625–4629. doi:10.1073/pnas.95.8.4625

Suri, C., P.F. Jones, S. Patan, S. Bartunkova, P.C. Maisonpierre, S. Davis, T.N. Sato, and G.D. Yancopoulos. 1996. Requisite role of angiopoietin-1, a ligand for the TIE2 receptor, during embryonic angiogenesis. *Cell*. 87:1171–1180. doi:10.1016/S0092-8674(00)81813-9

Sweeney, P., T. Karashima, S.J. Kim, D. Kedar, B. Mian, S. Huang, C. Baker, Z. Fan, D.J. Hicklin, C.A. Pettaway, and C.P. Dinney. 2002. Anti-vascular endothelial growth factor receptor 2 antibody reduces tumorigenicity and metastasis in orthotopic prostate cancer xenografts via induction of endothelial cell apoptosis and reduction of endothe-lial cell matrix metalloproteinase type 9 production. *Clin. Cancer Res*. 8:2714–2724.

Thomas, A.L., T. Trarbach, C. Bartel, D. Laurent, A. Henry, M. Poethig, J. Wang, E. Masson, W. Steward, U. Vanhoefer, and B. Wiedenmann. 2007. A phase IB, open-label dose-escalating study of the oral angio-genesis inhibitor PTK787/ZK 222584 (PTK/ZK), in combination with FOLFOX4 chemotherapy in patients with advanced colorectal cancer. *Ann. Oncol*. 18:782–788. doi:10.1093/annonc/mdl469

von Tell, D., A. Armulik, and C. Betsholtz. 2006. Pericytes and vascular stability. *Exp. Cell Res*. 312:623–629. doi:10.1016/j.yexcr.2005.10.019

Weis, J., and J.M. Schröder. 1989. Differential effects of nerve, muscle, and fat tissue on regenerating nerve fibers in vivo. *Muscle Nerve*. 12:723–734. doi:10.1002/mus.880120905

Weis, J., W. Dimpfel, and J.M. Schröder. 1995. Nerve conduction changes and fine structural alterations of extra- and intrafusal muscle and nerve fibers in streptozotocin diabetic rats. *Muscle Nerve*. 18:175–184. doi:10.1002/mus.880180205

Wong, A.L., Z.A. Haroon, S. Werner, M.W. Dewhirst, C.S. Greenberg, and K.G. Peters. 1997. Tie2 expression and phosphorylation in angio-genic and quiescent adult tissues. *Circ. Res*. 81:567–574.

Wood, J.M., G. Bold, E. Buchdunger, R. Cozens, S. Ferrari, J. Frei, F. Hofmann, J. Mestan, H. Mett, T. O'Reilly, et al. 2000. PTK787/ZK 222584, a novel and potent inhibitor of vascular endothelial growth factor receptor tyrosine kinases, impairs vascular endothelial growth factor-induced responses and tumor growth after oral administration. *Cancer Res*. 60:2178–2189.